

# **ORIGINAL RESEARCH**

# Single-cell Profiling of Intrahepatic Immune Cells Reveals an Expansion of Tissue-resident Cytotoxic CD4<sup>+</sup> T Lymphocyte Subset Associated With Pathogenesis of Alcoholic-associated Liver Diseases



Chao Gao, <sup>1,\*</sup> Shiguan Wang, <sup>2,3,\*</sup> Xiaoyu Xie, <sup>4,\*</sup> Pierluigi Ramadori, <sup>5,6,\*</sup> Xinying Li, <sup>3,\*</sup> Xiaoyu Liu, <sup>7</sup> Xue Ding, <sup>3</sup> Jinyuan Liang, <sup>3</sup> Bowen Xu, <sup>3</sup> Yawei Feng, <sup>3</sup> Xueying Tan, <sup>3</sup> Haoran Wang, <sup>3</sup> Yan Zhang, <sup>3</sup> Haiyan Zhang, <sup>8</sup> Tingguo Zhang, <sup>9</sup> Ping Mi, <sup>3</sup> Shiyang Li, <sup>7</sup> Cuijuan Zhang, <sup>9,10,§</sup> Detian Yuan, <sup>3,§</sup> Mathias Heikenwalder, <sup>5,6,§</sup> and Peng Zhang<sup>3,§</sup>

<sup>1</sup>Department of Hepatobiliary Surgery, General Surgery, Qilu Hospital, Cheeloo College of Medicine, Shandong University, Jinan, Shandong, China; <sup>2</sup>Department of Clinical Laboratory, Qilu Hospital of Shandong University, Jinan, Shandong, China; <sup>3</sup>Department of Biochemistry and Molecular Biology, School of Basic Medical Sciences, Cheeloo College of Medicine, Shandong University, Jinan, Shandong, China; <sup>4</sup>Department of Gastroenterology, Qilu Hospital of Shandong University, Jinan, Shandong, China; <sup>5</sup>Division of Chronic Inflammation and Cancer, German Cancer Research Center (DKFZ), Heidelberg, Germany; <sup>6</sup>University Tuebingen, Faculty of Medicine, Institute for Interdisciplinary Research on Cancer Metabolism and Chronic Inflammation, M3-Research Center for Malignome, Metabolome and Microbiome, Tübingen, Germany; <sup>7</sup>Advanced Medical Research Institute, Shandong University, Jinan, Shandong, China; <sup>8</sup>Department of Biochemistry, Heze Medical College, Heze, Shandong, China; <sup>9</sup>Institute of Pathology and Pathophysiology, Cheeloo College of Medicine, Shandong University, Jinan, Shandong, China; and <sup>10</sup>Department of Pathology, Qilu Hospital of Shandong University, Jinan, Shandong, China

#### **SUMMARY**

We identified a previously uncharacterized liver-resident CD4<sup>+</sup> T cell subset in the livers of patients with alcoholic-associated liver diseases compared with healthy and metabolic dysfunction-associated steatotic liver disease liver tissue. These CD4<sup>+</sup> T cells may play a pivotal immune pathogenic role in alcoholic-associated liver diseases.

**BACKGROUND & AIMS:** The immunological mechanisms underpinning the pathogenesis of alcoholic-associated liver disease (ALD) remain incompletely elucidated. This study aims to explore the transcriptomic profiles of hepatic immune cells in ALD compared with healthy individuals and those with metabolic dysfunction-associated steatotic liver disease (MASLD).

**METHODS:** We utilized single-cell RNA sequencing to analyze liver samples from healthy subjects and patients with MASLD and ALD, focusing on the immune cell landscapes within the liver. Key alterations in immune cell subsets were further validated using liver biopsy samples from additional patient cohorts.

**RESULTS:** We observed a significant accumulation of CD4 $^+$  T cells in livers of patients with ALD, surpassing the prevalence of CD8 $^+$  T cells, in contrast to patients with MASLD and healthy counterparts, whereas natural killer (NK) cells and  $\gamma\delta$ T cells exhibited reduced intrahepatic infiltration. In-depth transcriptional and developmental trajectory analyses unveiled that a distinct CD4 $^+$  subset characterized by granzyme K (GZMK) expression, displaying a tissue-resident signature and terminal effector state, prominently enriched among CD4 $^+$  T cells infiltrating the livers of patients with ALD. Subsequent examination of an independent ALD patient cohort corroborated the substantial enrichment of GZMK $^+$ CD4 $^+$  T lymphocytes, primarily within liver fibrotic zones, suggesting their potential involvement in disease progression. Additionally, we noted shifts in myeloid populations,

with expanded APOE<sup>+</sup> macrophage and FCGR3B<sup>+</sup> monocyte subsets in ALD samples relative to MASLD and healthy tissues.

**CONCLUSIONS:** In summary, this study unravels the intricate cellular diversity within hepatic immune cell populations, highlighting the pivotal immune pathogenic role of the GZMK<sup>+</sup>CD4<sup>+</sup> T lymphocyte subset in ALD pathogenesis. (*Cell Mol Gastroenterol Hepatol 2025;19:101411; https://doi.org/10.1016/j.jcmgh.2024.101411*)

*Keywords:* Alcoholic-associated Liver Disease; CD4<sup>+</sup> T Lymphocyte; Granzyme K; Metabolic Dysfunction-associated Steatotic Liver Disease; Single-cell RNA Sequencing.

\*Authors share co-first authorship; \$Authors share co-senior authorship.

Abbreviations used in this paper: ALCAM, activated leukocyte celladhesion molecule; ALD, alcohol-associated liver disease; ANOVA, analysis of variance; ASH, alcoholic steatohepatitis; CD4+ CTLs, cytotoxic CD4+ T lymphocytes; DAM, disease-associated microglia; DAPI, 4,6-diamidino-2-phenylindole; DE, differential expression; DEG, differentially expressed gene; FDA, United States Food and Drug Administration; GEMs, gel beads in emulsions; GSEA, Gene Set Enrichment Analysis; HCC, hepatocellular carcinoma; H&E, hematoxylin and eosin; HBV, hepatitis B virus; HRP, horseradish peroxidase; IF, immunofluorescence; IHC, immunohistochemistry; LAM, lipid-associated macrophage; L-R, ligand-receptor; LSD, least significant difference; MAIT, mucosa-associated invariant T; MASH, metabolic dvsfunction-associated steatohepatitis: MASLD, dysfunction-associated steatotic liver disease; MCD, methionine choline-deficient diet; MHC, major histocompatibility complex; MOAM, monocyte-derived alveolar macrophage; NET, neutrophil extracellular trap; NK, natural killer; PAGA, partition-based graph abstraction; PCA, principal component analysis; PCR, polymerase chain reaction; SCE-NIC, single-cell regulatory network inference and clustering; scRNAseq, single-cell RNA sequencing; UMI, unique molecular identifier.

Most current article

© 2024 The Authors. Published by Elsevier Inc. on behalf of the AGA Institute. This is an open access article under the CC BY-NC-ND license (http://creativecommons.org/licenses/by-nc-nd/4.0/).

2352-345X

https://doi.org/10.1016/j.jcmgh.2024.101411

lcohol-associated liver diseases (ALD) describes a wide range of liver disease entities caused by excessive alcohol consumption. Recent estimates suggest that about 1 million deaths per year from liver cirrhosis can be attributed to alcohol, with a rising incidence at an alarming rate.<sup>1,2</sup> The condition generally progresses from common hepatic steatosis to steatohepatitis, liver fibrosis, liver cirrhosis, and eventually hepatocellular carcinoma. 1,3,4 Earlier stages of ALD are considered reversible with abstinence from alcohol. For the treatment of alcoholic hepatitis, currently available drugs, such as corticosteroids,5 have a marginal short-term survival benefit, which is unsatisfactory for patients. However, for patients with end-stage ALD, the only curative therapy is liver transplantation.<sup>2,4</sup> To date, no pharmacological agent or treatment has been approved by the United States Food and Drug Administration (FDA) for the management of patients with ALD.6 Therefore, there remains an unmet need for the development of identification of new therapeutic targets and safer medical cures for the treatment of alcohol-induced liver disease.

Despite intense research efforts, mechanisms underlying ALD involved in the onset and progression remain elusive. The hepatic immune ecosystem contains many types of immune cells and involves a number of heterogeneous subpopulations. Multiple lines of evidence suggest that inflammation is very important for disrupted liver homeostasis in stress conditions generating from alcohol metabolism, and the immune microenvironment plays vital roles in the development of ALD at different stages. <sup>2,7-9</sup> A salient component in the development of ALD is Kupffer cell activation and recruitment of inflammatory monocytes and macrophages to the liver.8,10 Pro-inflammatory macrophages (M1) can drive the process of alcoholic liver injury via NF-κB signaling pathway.8 Alcohol feeding promotes an anti-inflammatory macrophage phenotype (M2) by regulating KLF4 expression.<sup>11</sup> Cho et al reported that alcohol could induce neutrophil extracellular trap (NET) formation that contributes to liver damage. Their work uncovered the heterogeneity of neutrophils in alcohol-associated hepatitis, including high-density and low-density neutrophils that show hyper-activated or exhausted transcriptomic profiles, respectively. Excessive alcohol use could also induce gut bacterial unbalance and elevate bacterial antigens and metabolites, causing depletion of circulating mucosa-associated invariant T (MAIT) cells that results in bacterial infection in patients with severe alcoholic hepatitis. 12 Nevertheless, the composition of liver immune cells in ALD and their contribution and interaction to the development of ALD is incompletely understood. Understanding the heterogeneity of immune cell types in ALD livers is essential to understand immune niche, which might be helpful to design effective immunotherapeutic strategies for the treatment of patients with ALD.

Single-cell RNA sequencing (scRNA-seq) is a powerful tool for the investigation of the cellular components and their interactions in the hepatic homeostatic and pathogenic microenvironment. Based on the computational methods of ligand-target links, scRNA-seq is able to provide insights into the intercellular crosstalk network. To date,

the study of scRNA-seq for gene-expression analyses in liver disease have been conducted in hepatic cirrhosis, <sup>14,16,18</sup> liver cancer, <sup>15</sup> non-alcoholic fatty liver disease/nonalcoholic steatohepatitis, <sup>19</sup> and chronic hepatitis B virus (HBV) infection. <sup>20</sup> A detailed definition of the functional heterogeneity and interaction of immune cell lineages would contribute to understand and identify specific immune cell subpopulations that involve in ALD pathogenesis.

To get a comprehensive depiction of the immunological mechanism within ALD pathogenesis, we applied scRNA-seq and constructed a landscape of hepatic immune cell atlas using livers from patients with ALD compared with healthy patients and patients with metabolic dysfunction-associated steatotic liver disease (MASLD). We identified a previously uncharacterized population of liver-resident CD4<sup>+</sup> T cell subset with a cytotoxic signature, which was specifically enriched in the hepatic fibrotic scope. These CD4<sup>+</sup> T cells are very likely to contribute to the pathogenesis of ALD and could be targeted in novel therapeutic approaches.

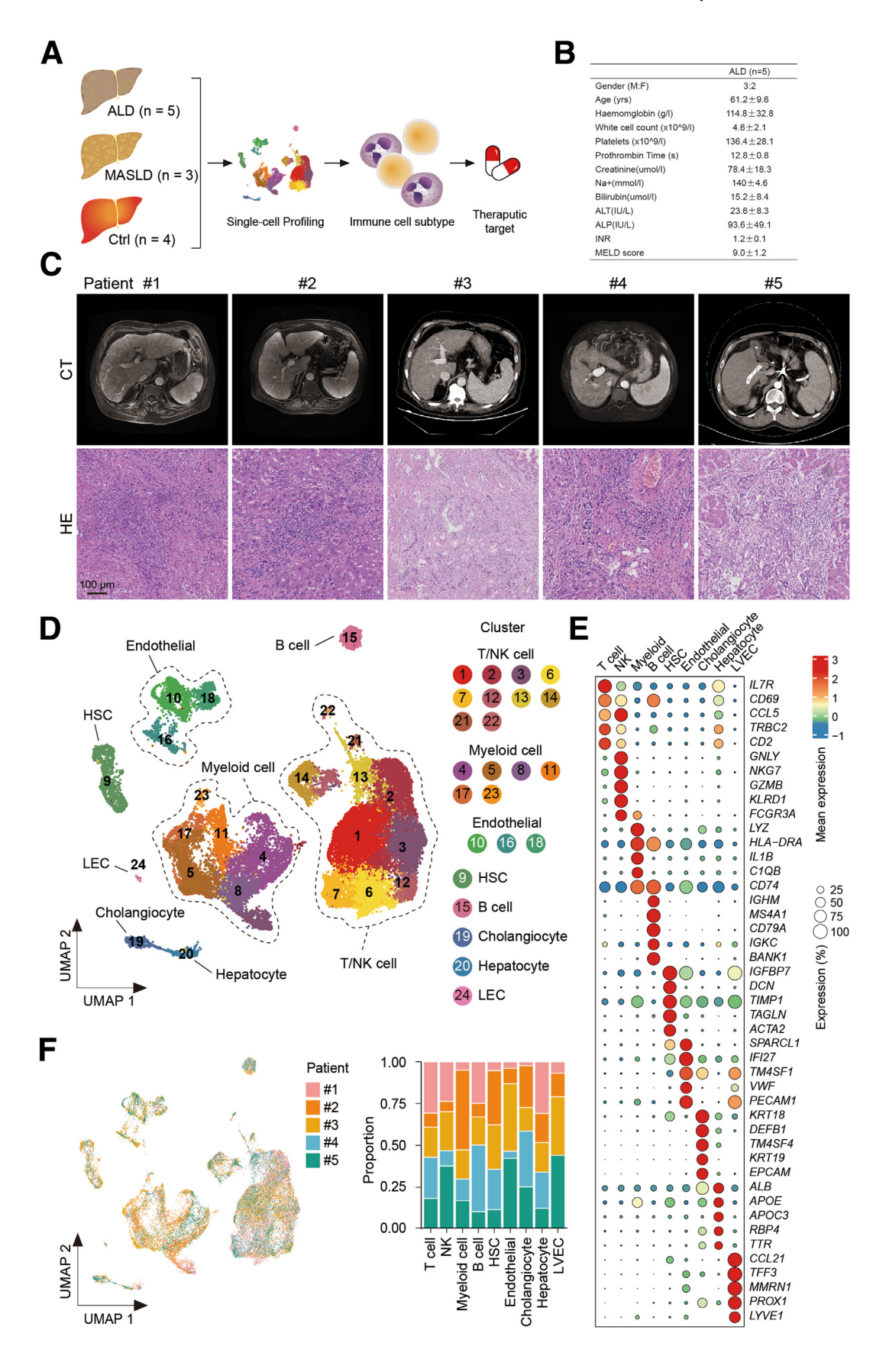
#### Results

# scRNA-seq Profiling of the Tissue Niche in Livers of Patients With ALD

We performed scRNA-seq on 5 fresh liver biopsies from ALD diagnosed patients (Figure 1A). Detailed clinical and pathological information are provided in Figure 1B and C. After rigorous quality control, we obtained 30,149 high-quality cells with an average of 1569 genes per cell profiled. All scRNA-seq data were merged, normalized, batch-corrected, and clustered to identify coarse cell types, including lymphoid, myeloid, endothelial, hepatic stellate cell, lymphoid endothelial cell, and liver parenchymal cells, including hepatocytes and cholangiocytes (Figure 1D and E). The major cell subsets were shared across all patients investigated (Figure 1F).

# Metabolically Responsive Signature of Proinflammatory Macrophage Subsets

To examine the extent to which the changes in the immune atlas may be specific to ALD, we pooled the immune cells in our cohort and in our recently published data on metabolic dysfunction-associated steatohepatitis (MASH),<sup>21</sup> and assess the differences in immune cell subsets at the single-cell level (Figure 2A). We first analyzed the myeloid cell compartments separately to facilitate exact cell type annotation. Clustering the myeloid-driven compartment resulted in 2 macrophage (Mφ-C1-APOE and Mφ-C2-FCGR3A), 3 monocyte (Mono-C1-FCGR3B, Mono-C2-FCGR3A, Mono-C3-CD14), and 2 dendritic (DC-C1-FCER1A and DC-C2-CLEC9A) as well as 1 cycling clusters (Figure 2B-C). Characteristic markers of different cell populations are labeled in Figure 2D. Although the difference did not reach statistical significance, a slight decrease in the proportion of dendritic cells can be observed (Figure 2C). DC-C1-FCER1A highly expressed FCER1A, CD1C, and CLEC10A, corresponding to cDC2,<sup>22</sup> whereas DC-C2-CLEC9A highly expressed CLEC9A, IRF8, CST3, and HLA-related genes, representing cDC1 (Figure 2E). cDC1 cells were



comparable in healthy, MASLD, and ALD livers (Figure 2F). cDC2 cells were higher in MASLD than in healthy or ALD samples (Figure 2B and Figure 2F), albeit not statistically significant, consistent with the previous reports that cDC2 are strongly associated with hallmarks of MASH in patients and the mouse models.  $^{23-25}$ 

When focusing on macrophages, while Mφ-C2-FCGR3A population corresponded to the classical M1 macrophage polarization, with expression of FCGR3A in the absence of CD163, Mφ-C1-APOE cells expressed both (Figure 2E), consistent with previous reports. 14,15 Expression of MARCO in Mφ-C1-APOE cells suggested that this subset was most likely derived from liver resident Kupffer cells<sup>26</sup> (Figure 2E). Examination of the 2 macrophage clusters revealed substantial population shifts, with Mφ-C1-APOE highly enriched and Mφ-C2-FCGR3A reduced in livers from patients with ALD, albeit not statistically significant (Figure 2G and Figure 3A). Differential gene expression analysis revealed a transcriptional signature of APOE, C1QA, C1QB, C1QC, APOC1, CTSD, CTSB, CTSL, FABP5, LAMP1, LIPA, and LGALS3 in Mφ-C1-APOE, signatures associated with lipid metabolism $^{27-29}$  and phagocytosis (Figure 3*B*–*C*). The lipid metabolism signature of Mφ-C1-APOE is reminiscent of "lipid-associated macrophage" (LAM) previously defined in the context of obesity and the "disease-associated microglia" (DAM) found in the context of Alzheimer's disease.<sup>30</sup> This remarkable similarity suggested a conserved macrophage response signature present across different tissues in response to aberrations in lipid metabolism. In addition to the lipid metabolism signature up-regulated in Mφ-C1-APOE (Figure 3D), functional analysis by Gene Set Enrichment Analysis (GSEA) further identified a stronger immune signature for M $\phi$ -C1-APOE (Figure 3*E*-*G*). Notably, M $\phi$ -C1-APOE expressed a set of pro-inflammatory genes including VSIG4, CCL3, IL18, CCL4L2, and CCL4 but not IL1B (Figure 3H-L), analogous to the LAM and DAM mentioned above. These data highlighted M $\phi$ -C1-APOE subset as a metabolically responsive macrophage population with proinflammatory functions during ALD progression.

#### Diversity Within the Monocyte Populations

Heterogeneous monocyte populations consisted of 3 subsets (Mono-C1-FCGR3B, Mono-C2-FCGR3A, Mono-C3-CD14) (Figure 4A). Mono-C3-CD14 highly expressed *CD14* in the absence of CD16 (LYZ<sup>+</sup>CD14<sup>++</sup>CD16<sup>-</sup>) (Figure 4A), a signature of classical monocytes.<sup>31</sup> Two additional non-classical monocyte subsets (LYZ<sup>+</sup>CD14<sup>+</sup>CD16<sup>+</sup>) were distinguished by the expression of the CD16 isoforms *FCGR3B* and *FCGR3A* among other differentially expressed genes, and were thereafter referred to as Mono-C1-FCGR3B and Mono-C2-FCGR3A (Figure 4B), respectively. Mono-C1-

FCGR3B showed a trend toward upregulation in ALD (Figure 4C). We performed differential expression (DE) and pathway analysis to determine subset-specific gene programs (Figure 4D). Compared with the classical monocytes of the Mono-C3-CD14 subset, Mono-C2-FCGR3A is enriched in IFN $\gamma$ -mediated signaling, as well as genes involved in antigen processing and presentation (Figure 4D–E). In contrast, Mono-C1-FCGR3B exhibits a pro-inflammatory pattern of gene expression, including overexpressed genes regulating cellular response to lipopolysaccaride, unfolded protein, and temperature stimulus (Figure 4D–E). Of particular note, this FCGR3B<sup>+</sup> monocyte population closely resemble a most recently defined subset of monocytederived alveolar macrophages (MoAMs) in patients with severe COVID-19.

We next performed the trajectory analysis to infer changes in the status of monocyte subsets. We identified 2 transformations: Mono-C3-CD14 to Mono-C1-FCGR3B (Trajectory 1) and Mono-C3-CD14 to Mono-C2-FCGR3A (Trajectory 2) (Figure 5A). Several pro-inflammatory molecules, including *PTGS2*, *CXCL8*, *PLAUR*, and *CCL4L2*, were upregulated along the Mono-C1-FCGR3B axis, whereas *CD74* and *CLEC10A*, implicated in antigen processing, were upregulated along the Mono-C2-FCGR3A axis (Figure 5B). Importantly, Mono-C1-FCGR3B represented the major source for *CXCL8* production (Figure 5C), indicative of its potential role in inflammatory response and tissue injury (Figure 5D).

# CD4<sup>+</sup> T Cell Population Expansion in Livers of Patients With ALD

We next focused our analysis on the detailed changes of T cells/natural killers (NKs) subsets (Figure 6A). The reclustering of T cells/NKs obtained 6 major cell clusters according to the expression and distribution of canonical T cell markers , including CD4+ T cells ( $CD3D^+CD4^+$ ), CD8+ T cells ( $CD3D^+CD4^+$ ), NKT cells ( $CD3D^+NKG7^+$ ), NK cells ( $NKG7^+GNLY^+$ ),  $\gamma\delta$  T cells ( $CD3E^+TRDC^+$ ), and 2 clusters exhibiting a heat-shock stress-activated pathway (Figure 6A-C), as indicated by expression of HSP family members (HSPA1A, HSPB1, HSPD1, and HSPA6), as previously reported. One cluster could not be explicitly identified because of a lack of specific markers. Based on the top differentially expressed genes (DEGs), we identified unique markers for all subsets (Figure 6D-E).

Comparison of the abundance of each individual T cell cluster showed a dramatic loss of NK cells and an expansion of CD4<sup>+</sup> cell in ALD samples (Figure 7*A*–*B*). Notably, the 3 NK subsets (NK-C1-GNLY, NK-C2-CCL4, NK-C3-PTGDS) showed the same decreased trend in ALD samples (Figure 7*C*), indicating global rather than subset-specific

Figure 1. (See previous page). Single-cell transcriptome map of cell types in livers from patients with ALD. (A) Diagram illustrating the overall study design. (B) Information on the patients with ALD included in this study. (C) Computed tomography images and H&E staining of human livers obtained from the 5 patients with ALD included in the scRNA-seq analysis. (D) UMAP plots displaying major cell types identified in the livers of the 5 individuals with ALD, encompassing 24 clusters. (E) Bubble heatmap illustrating the gene expression patterns within major cell clusters. (F) UMAP plots presenting major cell clusters (left panel) and bar plots representing the proportion of cell types across patients (right panel).

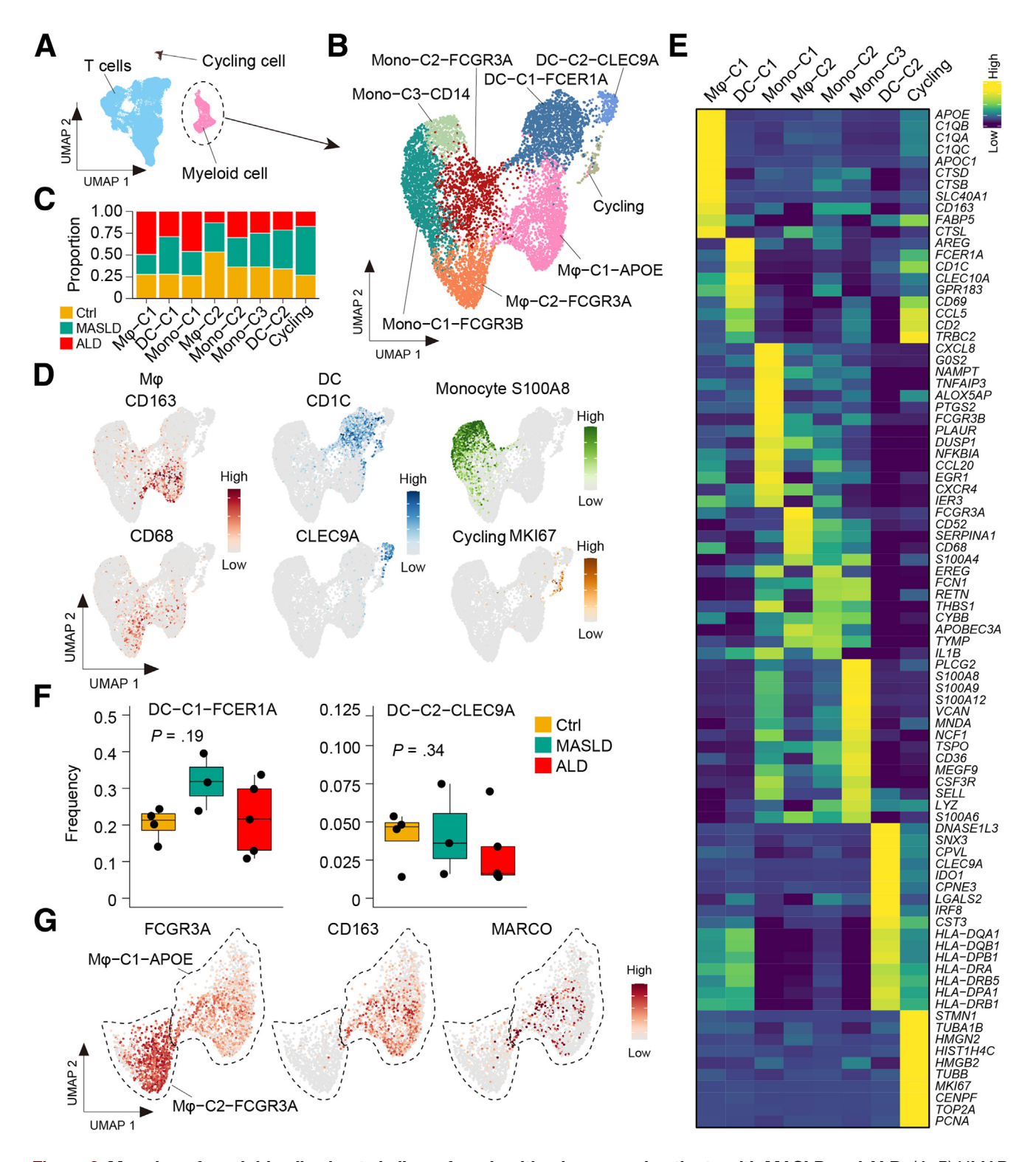


Figure 2. Mapping of myeloid cell subsets in livers from healthy donors and patients with MASLD and ALD. (A–B) UMAP plots displaying major immune cell clusters obtained from integrated datasets of healthy donors and individuals with MASLD and ALD (A). Myeloid cells were highlighted and subjected to re-clustering (B). (C) Bar plots indicating the proportion of myeloid cell subsets in liver donors. (D) Heatmap displaying the 2 macrophage subsets in liver donors. (E) Heatmap displaying the expression levels of marker genes within each myeloid cell subset. (F) UMAP plots showing the expression of single marker genes in the 2 macrophage subsets. (G) UMAP plots demonstrating the expression levels of specific marker genes within 2 macrophage subsets.

6

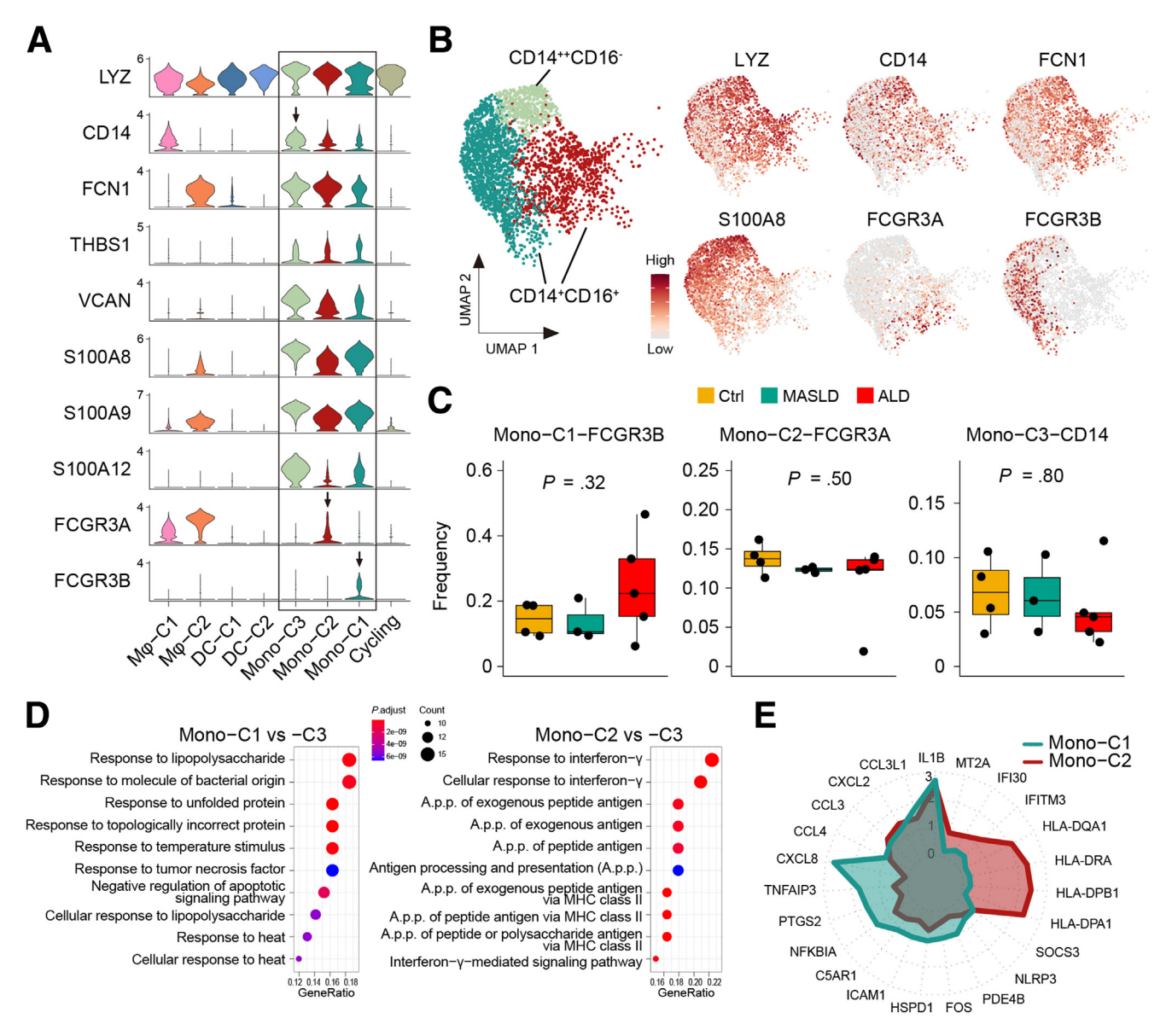


Figure 4. Mapping of monocyte cell subsets in livers from healthy donors and patients with MASLD and ALD. (A) Violin plots representing the differentially expressed marker genes within the monocyte cell subsets. (B) UMAP plots displaying the expression levels of specific marker genes within the monocyte subsets. (C) Box plots indicating the proportions of the 3 monocyte cell subsets in liver donors. Data are shown in mean  $\pm$  SEM; P-value was obtained by Student's t-test. (D) DE and pathway analysis revealing subtype-specific gene programs. (E) Radar plot showing the scaled expression levels of the indicated genes.

reduction of NK cells. IHC staining using the NK cell marker NCR1 further confirmed decreased proportion of NK cells in liver samples from ALD cases as compared with control and

MASLD (Figure 7*D*). Besides NK cells, cells of  $\gamma\delta$ -C2-CMC1,  $\gamma\delta$ -C4-VCAM1, and CD8-C2-NKG7 subsets were also reduced (Figure 7*C*). Immunofluorescence (IF) staining of CD8 and

Figure 3. (See previous page). Immunological features of macrophage subsets. (A) Heatmap displaying the 2 macrophage subsets in liver donors. (B) UMAP plots showing the expression of single marker genes in the 2 macrophage subsets. (C) Bar plots depicting the proportion of the 2 macrophage subsets in liver donors. One-way ANOVA followed by Fisher's LSD test to provide a clearer comparison between each group. (D) UMAP plots exhibiting the expression levels of individual marker genes. (E-H) GSEA analysis of the indicated gene sets, comparing the 2 macrophage subsets. (I) Ranking of DEGs in the 2 macrophage subsets. (J) Bar plots illustrating the expression differences of genes in the 2 macrophage subsets. Data are shown in mean  $\pm$  SEM; \*\*\*\*\*P < .0001 by Student's t-test. (K) Bar plots showing the expression difference of pro-inflammatory genes in the 2 macrophage subsets.

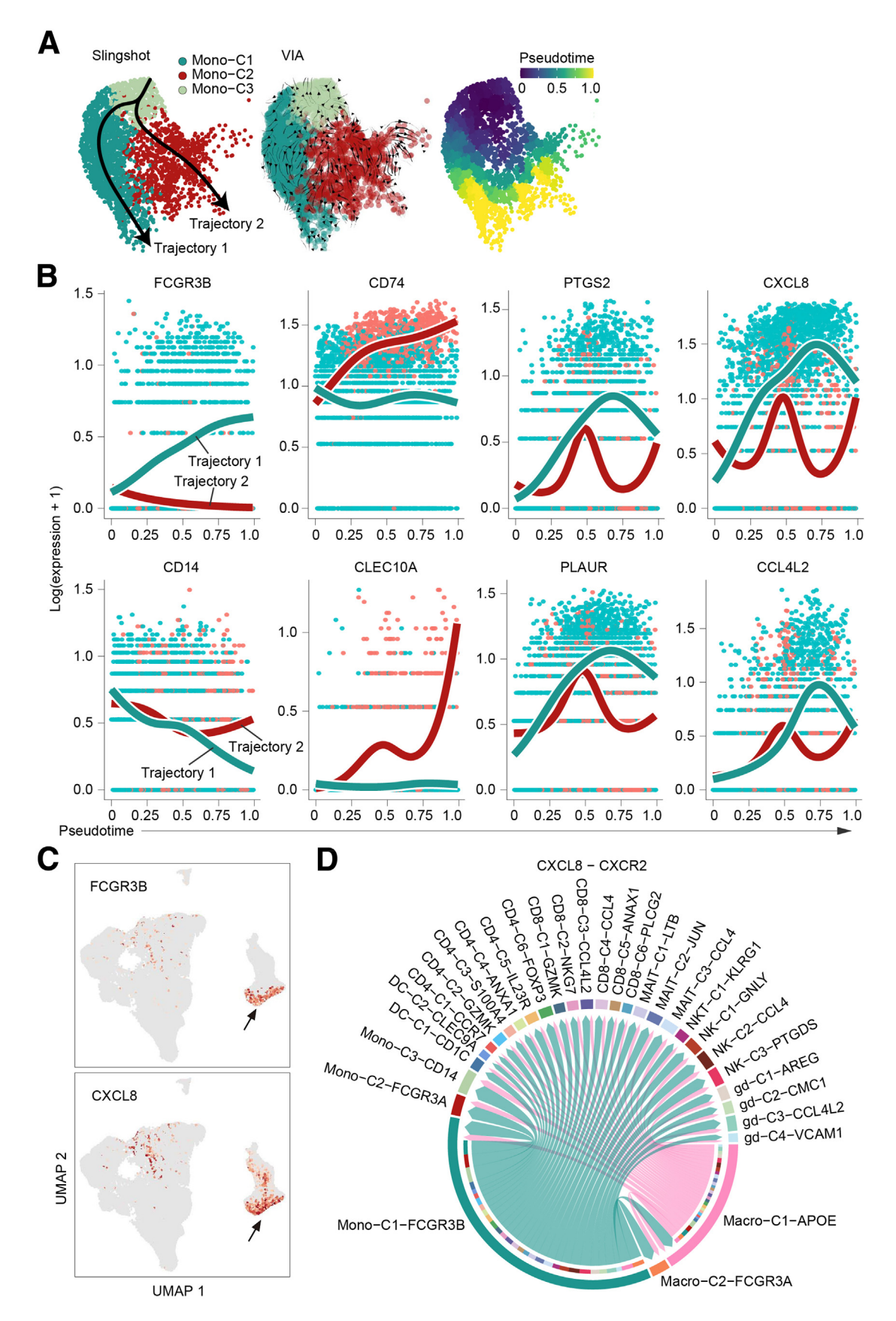
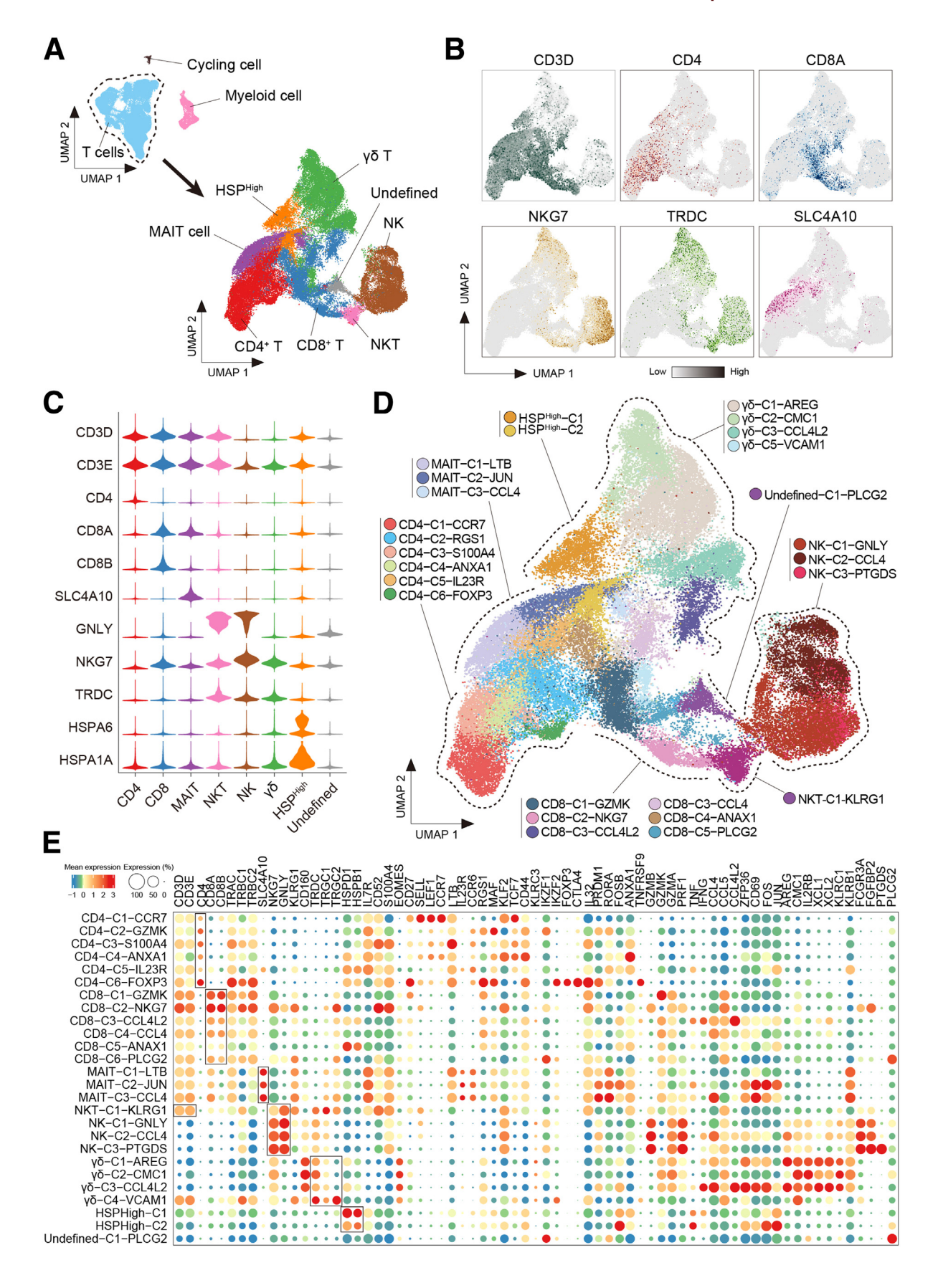


Figure 5. Immunological features of monocyte cell subsets. (A) Visualization of the monocyte trajectories inferred by Slingshot and VIA. The color map on the right represents pseudotime, ranging from early (purple) to late (yellow). (B) Expression of the indicated genes along the pseudotime axis. (C) UMAP plots illustrating the correlated expression of pro-inflammatory genes in monocyte cell subsets. (D) CSOmap showing the correlation of the CXCL8-CXCR2 L-R pair among immune cell subsets.



NKG7 confirmed marked reduced of CD8<sup>+</sup>NKG7<sup>+</sup> T cells in livers from ALD cases (Figure 7E). A total of 6 CD4 $^+$  T-cell clusters were identified, including naive (CD4-C1-CCR7), effector memory (CD4-C2-GZMK), memory-like (CD4-C2-S100A4), central memory (CD4-C4-ANXA1), T<sub>H</sub>17 (CD4-C5-IL23R), and regulatory (CD4-C6-FOXP3) T cells (Figure 7C). The 9 subsets of CD8<sup>+</sup> T cell clusters included 2 effector CD8<sup>+</sup> T cell subsets (CD8-C1-GZMK and CD8-C2-NKG7), 2 memory (CD8-C3-CCL4L2 and CD8-C4-CCL4) subsets, central memory (CD8-C5-ANXA1) subset, 1 subset characterized by high expression of PLCG2 (CD8-C6-CCL4L2), and 3 subsets of MAIT cells (MAIT-C1-LTB, MAIT-C2-JUN and MAIT-C3-CCL4), sharing expression of SLC4A10 (Figure 7C). IF staining for CD4, CD8, and ANXA1 revealed a significant expansion of the central memory T cell subset (CD4-C4-ANXA1) and a slight expansion in the central memory CD8 T cell subset (CD8-C5-ANXA1) in ALD liver samples compared with control and MASLD (Figure 7*E*). The 3 subsets of NK cell clusters were defined as NK-C1-GNLY, NK-C2-CCL4, and NK-C3-PTGDS subsets.<sup>20</sup> The 4 subtypes of  $\gamma\delta$  T cells included  $\gamma\delta$ -C1-AREG,  $\gamma\delta$ -C2-CMC1,  $\gamma\delta$ -C3-CCL4L2, and  $\gamma\delta$ -C4-VCAM1 subsets. <sup>34,35</sup>

Focusing on the CD4<sup>+</sup> and CD8<sup>+</sup> T cells, we identified increased proportion of CD4<sup>+</sup> T cells were found in the samples from ALD as compared with control and MASLD, and we also observed CD4<sup>+</sup> T cells mainly localized in the fibrotic zone (Figure 7*D*). CD8<sup>+</sup> T cells show an increased trend in ALD but did not reach statistical significance as compared with control and MASLD (Figure 7*D*). The numbers of CD4<sup>+</sup> T cells and CD8<sup>+</sup> T cells do not differ between MASLD and healthy cases, in line with the data on MASH and control groups from report by Ma et al.<sup>36</sup>

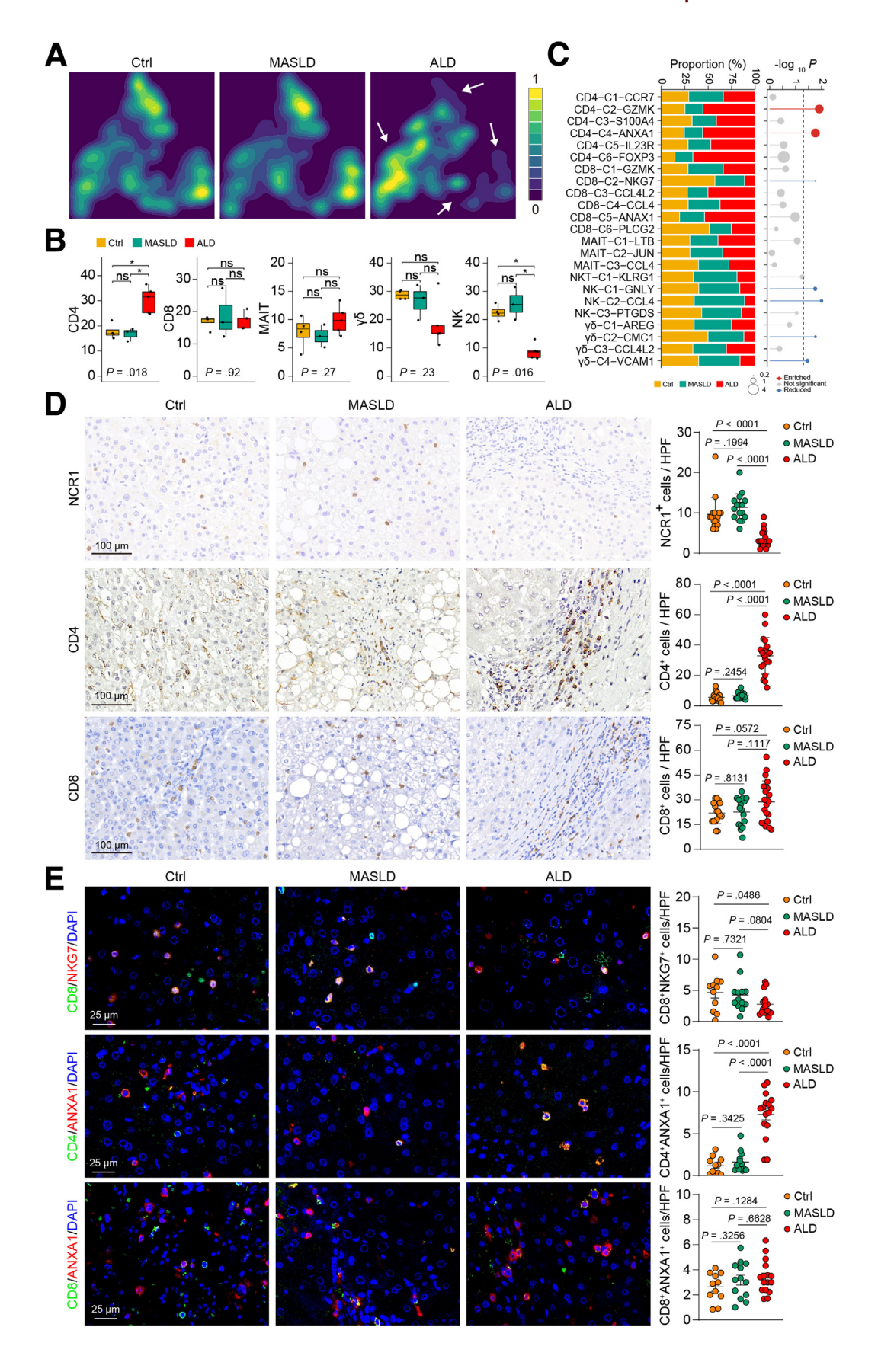
# Tissue-resident GZMK<sup>+</sup>CD4<sup>+</sup> T Cells Enrichment in Livers of Patients With ALD

Quantification of the relative percentage of each CD4<sup>+</sup> T cell subset revealed that the CD4-C2-GZMK and CD4-C4-ANAX1 subsets were expanded in livers from patients with ALD (Figure 7*C*), of which the CD4-C2-GZMK subset was most prominently upregulated. Representative highly expressed genes in the CD4-C2-GZMK subset include those well-documented in T cell activation/differentiation (eg, *IKZF3*, *MAF*, *BATF*)<sup>37</sup>, and effector function (eg, *GZMK*, *GZMB*, *GZMM*), whereas genes involved in T cell stemness/quiescence (eg, *CCR7*, *SELL*, *LEF1*)<sup>20</sup> were expressed at low levels (Figure 8*A*–*B*). The CD4-C2-GZMK subset also showed features of tissue residency, including the relatively high expression of surface receptor CD49A (encoded by *ITGA1*) and *CXCR4*, as well as the master transcription factor for tissue residency *ZNF683* (Figure 8*B*). These features suggest

that they represent tissue-resident cytotoxic CD4 T cells. Indeed, the transcriptional features of the CD4-C2-GZMK subset was analogous to a group of granzyme A-producing  $\mathrm{CD4}^+$  T cells implicated in acute graft-vs-host disease. <sup>37</sup>

We next applied unsupervised inference method Monocle and partition-based graph abstraction (PAGA) analysis 15 to construct the potential developmental trajectories of CD4<sup>+</sup> T cells (Figure 8C), excluding T<sub>H</sub>17 cells of CD4-C5-IL23R as they were distantly segregated from the other subsets. Both analyses showed that the CD4-C1-CCR7 cells were at the beginning of the trajectory path, whereas the CD4-C2-GZMK and CD4-C6-FOXP3 cells were at the different terminal states (Figure 8D). We next investigated the transcriptional changes associated with transitional states. Genes implicated in T cell differentiation and effector function were increased gradually along the trajectory (Figure 8D). Also, the expression of the HVEM receptor CD160, ITGA1, CXCR4, and CXCR6, as well as the master transcription factor for tissue residency ZNF683,38 showed the same trend, implying that the tissue residency programs were activated along with terminal effector differentiation in the CD4-C2-GZMK subset (Figure 8D). CD4-C3-S100A4 and CD4-C4-ANXA1 cells located in the middle of the trajectory and were enriched for genes in the NF-κB signaling and AP-1, in line with their intermediate activation state. The Treg markers and effectors were also co-expressed, including the expression of IL32, which has been recently reported as key regulators of Treg cell development<sup>35</sup> (Figure 8D). By integrating the trajectory information, this transition was determined to initiate with CD4-C1-CCR7 cells, through an intermediate activation state characterized by CD4-C3-S100A4 and CD4-C4-ANXA1 cells, and finally reach either an effector state of CD4-C2-GZMK cells, or a regulatory state of CD4-C6-FOXP3 cells (Figure 8D). By analyzing the trajectories of CD4<sup>+</sup> T cells in control, MASLD, and ALD cases separately, we confirmed that CD4-C2-GZMK cells were substantially enriched in livers of patients with ALD (Figure 8E). Pathway analysis further confirmed that genes increased along the trajectory were related to allograft rejection, indicative of the roles of CD4-C2-GZMK cells in mediating tissue damage (Figure 8F). Using serial section of liver tissue samples on immunohistochemistry (IHC) staining of CD4 and GZMK, we found a similar distribution and expansion trend between GZMK<sup>+</sup> cells and CD4<sup>+</sup> cells in livers of patients with ALD as compared with livers of patients with MASLD and healthy donors (Figure 8G). Dual IF staining of CD4 and GZMK further confirmed marked expansion of these double-positive T cells in livers from ALD cases in the fibrotic septa (Figure 8H), probably reflecting its immune-pathogenic features associated with ALD pathogenesis.

Figure 6. (See previous page). Mapping of lymphocyte cell subsets in livers from healthy donors and patients with MASLD and ALD. (A) UMAP plots illustrating the major immune cell clusters obtained from integrated datasets of healthy donors and individuals with MASLD and ALD. The lymphocyte population was re-clustered, resulting in the identification of 8 distinct NK & T-cell subsets. (B) UMAP plots displaying single gene expression levels of specific marker genes within the identified NK & T-cell subsets. (C) Violin plots representing the DE of marker genes within the NK & T-cell subsets. (D) UMAP plots revealing 26 subclusters within the NK & T-cell subsets. (E) Bubble heatmap displaying the gene expression patterns within the 26 NK & T-cell subsets.



## Gene Regulatory Networks Involved in CD4<sup>+</sup> T Cell Subsets

We next used single-cell regulatory network inference and clustering (SCENIC) to map the gene regulatory networks governing these CD4<sup>+</sup> T cell states. 40 Marked differences in regulon activity between each subset were observed (Figure 9A). As expected, the CD4-C6-FOXP3 cluster had the highest regulon activity for FOXP3, whereas specific to the CD4-C1-CCR7 cluster were the TCF7 and LEF1 regulons (Figure 9A–C). Besides the key transcription regulators that previously known to be associated with T cell differentiation and functionality, including IKZF1 and RORA, SCENIC analysis identified KLF13 and KMT2A with high regulon specificity in CD4-C2-GZMK cells. These data are highly relevant, given that KLF13 has been demonstrated to cooperate with c-Maf to regulate IL-4 expression in Th2 cells. 41 KLF13 has also been shown to correlate with the cytotoxic program in CD8<sup>+</sup> T cells. 42 KMT2A plays crucial roles for the retention of cytokine production, specifically in memory Th2 cells.<sup>43</sup> These TFs were inferred to regulate a network of genes implicated in critical functions of T cells (Figure 9C), pointing to them as driving forces of the development of CD4-C2-GZMK cells, although this should be further verified.

## Cell-cell Communication Analysis Among Immune Cell Subsets

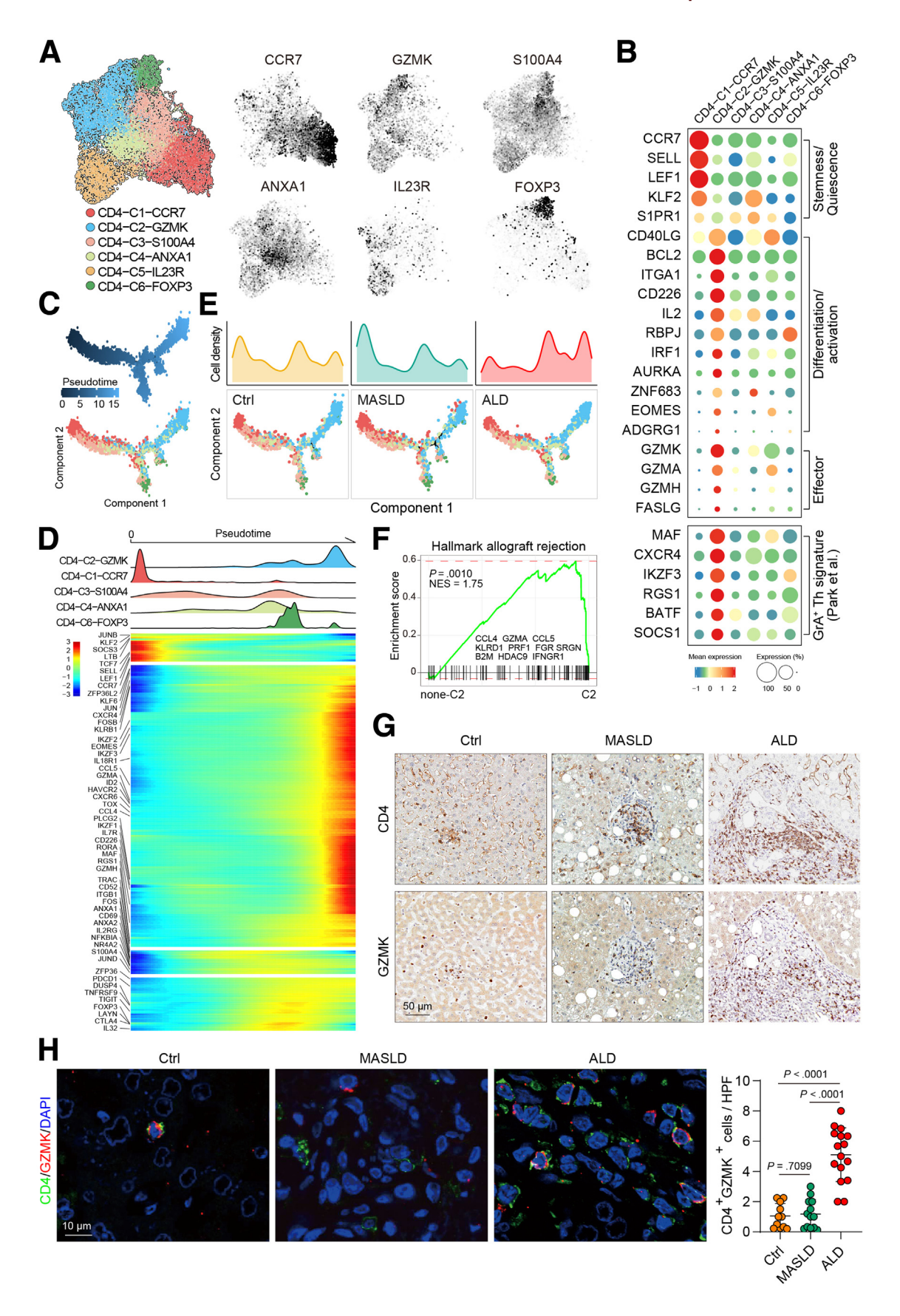
To gain insights into the regulatory relationships among cell subsets, we utilize immune-related ligand-receptor (L-R) pairs to calculate the strengths of the interactions.<sup>44</sup> Comparison of the overall communication probability across the 3 conditions revealed that IL1 and TNF signaling pathways were highly active in livers from patients with ALD (Figure 10A-C), with the myeloid cells as the main signal receivers (Figure 10B-D). Focusing on the cytotoxic CD4<sup>+</sup> T cells, the CD4-C2-GZMK subset from all 3 conditions showed strong potential interaction via the TCR signaling and the co-stimulator CD28/B7 family CD86-CD28 (Figure 10D), consistent with their fundamental roles in mediating T cell activation. Pathways through KLRB1, CD6, and CD55 were specifically active in livers from patients with ALD (Figure 11A-E). KLRB1 is reported to play both co-stimulatory and co-inhibitory roles in T cells. 45-47 Of note, KLRB1 has recently been reported to mark the cytotoxic CD4<sup>+</sup> T cells.<sup>48</sup> CD6 is a co-stimulatory receptor expressed on T cells that binds activated leukocyte celladhesion molecule (ALCAM), modulating effector T cell activation and trafficking. 49,50 ADGRE5/CD55 interaction drives CD4+ T cell activation, expansion, and function, comparable with CD28 costimulation.<sup>51,52</sup> The stronger interactions via KLRB1, CD6, and CD55 suggest that these pathways might contribute to the expansion of the CD4-C2-GZMK subset, which may drive disease pathogenesis in ALD.

## **Discussion**

In this study, we applied single-cell sequencing to characterize the hepatic immune cell atlas of ALD. Our findings highlight a distinct population of GZMK-producing CD4 $^{+}$  T cells exhibiting a terminal effector state and liver-resident signature that is the prominently enriched CD4 $^{+}$  T cell population and particularly localizes within the fibrotic livers of patients with ALD as compared to individuals with MASLD and healthy controls. In myeloid populations, a significant shift in the composition is noted, with an expansion of APOE $^{+}$  macrophages and FCGR3B $^{+}$  monocytes. These observations provide further insights into the immunopathogenesis of ALD in humans.

CD4<sup>+</sup> T cells have been extensively studied in a range of etiologies of liver fibrosis such as MASLD, 14,36 MASH, 16 and alcoholic steatohepatitis (ASH),14 but many gaps remain regarding their potential role in immune-mediated fibrosis. More recently, the roles of CD4<sup>+</sup> T cells during the progression from MASLD to MASH have been investigated at a single-cell level by Woestemeier et al, showing that CD4<sup>+</sup> T cells with a T<sub>H</sub>17 polarization state are enriched in the fibrotic livers of patients with MASH compared with patients with MASLD.<sup>16</sup> Work of Ma and coworkers also report CD4<sup>+</sup> T lymphocytes characterized by producing more IL-17 in methionine choline-deficient diet (MCD)-induced MASLD mice.33 Our current data have identified 6 human CD4+ T cell populations, that are naive (CD4-C1-CCR7), effector memory (CD4-C2-GZMK), memory-like (CD4-C2-S100A4), central memory (CD4-C4-ANXA1), and TH17 (CD4-C5-IL23R) and regulatory (CD4-C6-FOXP3) T cells. Interestingly, we also find that the number of these T<sub>H</sub>17 cells increases in patients with ALD compared with patients with MASLD and healthy humans. Moreover, our integration on developmental trajectories reports here that this T<sub>H</sub>17 (CD4-C5-IL23R) subset is distantly segregated from the other CD4+ T cell subsets we have clustered in our data. Another single-cell level report by Ramachandran et al shows that one CD4<sup>+</sup> T cell subset reduces significantly, whereas the other subset increases significantly in liver cirrhosis cohorts by combining ALD and MASLD samples when compared with healthy control samples according to their annotation. 14 Interestingly, among the 6 subsets in our data, the naive (CD4-C1-CCR7) subset is reduced and the other 5 subsets are increased in patients with ALD, which

Figure 7. (See previous page). Up-regulated infiltration of CD4<sup>+</sup> T cells in livers from patients with ALD. (A) Heatmap showing the altered cell abundance in ALD samples compared with healthy and MASLD samples. (B) Box plots illustrating the proportions of NK & T-cell subsets in the livers of 3 different donors. The Wilcoxon test was used to analyze differences between groups. (C) Bar plots indicating the proportions of 5 NK & T-cell subclusters in the livers of different donors. (D) IHC staining and quantification of NK, CD4, and CD8 in the 3 types of liver samples. (E) Representative photomicrographs of the human liver tissue sections from healthy donors (Ctrl) and patients with MASLD and ALD after IF staining with antibodies against CD8 (green) and NKG7 (red), CD4 (green) and ANXA1 (red), CD8 (green) and ANXA1 (red). For B and D-E, data are shown in mean ± SEM; P-value was obtained by Student's t-test.



might be in line with the widely different 2 populations described by Ramachandran et al.  $^{14}$ 

In recent years, cytotoxic CD4+ T lymphocytes (CD4+ CTLs) have been repeatedly characterized in humans and mice. 16,37,48,53,54 Hashimoto et al reported that GZMB+CD4+ T cells were quite abundant in supercentenarians. CD4<sup>+</sup> CTLs extracted from supercentenarians could produce IFN- $\gamma$  and TNF- $\alpha$  upon ex vivo stimulation.<sup>48</sup> A single-cell transcriptome sequencing study has identified infiltrating CD4+ CTLs in human bladder cancer, 55,56 where they could directly kill tumor cells in a major histocompatibility complex (MHC) class II-dependent manner, suggestive of their important role in immunosurveillance. Another potential function of CD4<sup>+</sup> CTLs is antiviral immunity, in which their cytotoxic effector mechanisms, the Fas ligand (CD95L) and Perforin (PFP)/Granzyme-dependent pathways, are important for cell-mediated killing. 53 However, the understanding of the pathophysiological role of CD4<sup>+</sup> CTLs remains incomplete, particularly in the context of the conversion from CD4<sup>+</sup> helper T cells to CD4<sup>+</sup> CTLs. Our scRNA-seq analysis suggests that subset of CD4<sup>+</sup> CTLs, GZMK<sup>+</sup>CD4<sup>+</sup> T cells is significantly enriched in livers from patients with ALD. Histological data also reveal its role associated with hepatic fibrosis. We describe here that these GZMK<sup>+</sup>CD4<sup>+</sup> T cells are in a terminal effector differentiation, particularity involving immune regulation such as allograft rejection, IL6/Jak/STAT3 signaling, IFNγ response, and TNF signaling, indicative of the roles in mediating inflammation and tissue damage. These findings in ALD suggest that cytotoxic CD4+ T lymphocytes might have a pathogenic function. Further functional experimental studies are warranted to investigate its detailed expression profiles and functions in ALD, as well as other pathologies featured by fibrosis and tissue damage.

In contrast to marked expansion of CD4<sup>+</sup> T cell subsets in patients with ALD, NK cells are the most reduced liverinfiltrating subsets in ALD cases in our analysis, containing all the NK subsets (NK-C1-GNLY, NK-C2-CCL4, NK-C3-PTGDS). NK cells, a key component of innate immunity, are much known to be functionally impaired due to the oxidative breakdown of alcohol and acetaldehyde in the progression of ALD.<sup>57</sup> In the mouse model of ALD,<sup>58</sup> chronic ethanol feeding significantly reduces the numbers of intrahepatic NK cells and suppresses their killing capacity on activated HSCs that are responsible for fibrogenesis. In the liver of patients with severe alcoholic hepatitis, studies have reported reduction of activated NK cells,<sup>59</sup> and impairment on their cytotoxic functions diminish the expression of IFN- $\gamma$  as well as IFN- $\gamma$ -activated signal pathway, which leads the limitation upon IFN- $\gamma$ -induced cell cycle arrest and apoptosis that thus accelerates liver fibrosis.<sup>60</sup> Our study

incisively strengthened this notion that the numbers of cytotoxicity NK cells were significantly reduced in livers of patients with ALD as analyzed by subpopulation statistics. This observation is in line with the fact that patients with ALD display a reduction of NK cells, resulting in a decrease in antiviral, anti-fibrotic, and anti-tumor effects of NK cells, thereby contributing to an increased susceptibility to viral hepatitis and an accelerated progression of liver fibrosis and hepatocellular carcinoma (HCC) in patients with ALD.<sup>61</sup>

Recent publications emphasize on the infiltration of myeloid-derived cells could foster ALD, but the involved mechanism is not clearly defined, especially for macrophages and monocytes. Under physiological conditions, it was reported that the role of polarized macrophages within tissues was regulated by various signals derived from microenvironment.<sup>62</sup> Our study defined APOE<sup>+</sup> tissueresident macrophages as a group of ALD unique lipidassociated contrast with macrophages in Gpnmb<sup>+</sup>Spp1<sup>+</sup> counterparts in healthy subjects and patients with MASH,63,64 which might be shaped by molecular patterns from lipid overload hepatocytes induced by alcohol. Accordingly, the primary function of this special macrophage population is to engulf and remove the damaged tissue; thereafter, a battery of cytokines and chemokines may recruit and evoke other immune cells for further responsive process.<sup>65</sup> CD14<sup>+</sup>FCGR3B<sup>+</sup> monocyte subtypes, as a specific population responding to gut-derived endotoxin, were involved in the aforementioned process. Current single-cell transcriptome data show that FCGR3B gene expression also increases significantly in CCL3L1positive non-classical monocytes in severe COVID-19 cases, 32,66 indicating conserved response signature across different tissues and disease. Notably, CD14+FCGR3B+ monocytes were the major source of CXCL8 production in the liver in humans with ALD, and they may in turn interact and promote the activation of immune cells through CXCL8-CXCR2 axis, thereby exacerbating ALD progression. Additionally, recent studies demonstrated that CXCL8 can also interact with activated endothelial cells, which potentially facilitate leukocyte recruitment and infiltration in heart failure<sup>67</sup> and cirrhosis.<sup>68</sup> Considering CD14<sup>+</sup>FCGR3B<sup>+</sup> monocytes as the hub cells in intercellular interaction network, inhibiting CXCL8 might be a possible future immunotherapy approach to ALD.

In summary, we report a remarkably expanded effector population of  $CD4^+$  CTLs in livers from ALD-related patients. This population specifically enriched in liver fibrotic zones seems to have an inflammation regulatory function, reflecting their roles in ALD immunopathogenesis. These findings not only improve our understanding of hepatic immunological components in the context of ALD, but also

Figure 8. (See previous page). Characteristics of  $GZMK^+CD4^+$  T cell subset. (A–B) UMAP plots (A) and bubble heatmap (B) showing the expression levels of specific marker genes within 6 CD4+ T cell subsets. (C) Developmental trajectories of the CD4+ T cell subsets. (D) Feature genes along the developmental trajectories. (E) Developmental trajectories of the CD4+ T cell subsets in healthy donors (Ctrl) and MASLD and ALD samples. (F) GSEA on CD4-C2-GZMK showing enrichment of the allograft rejection pathway. (G) IHC staining of GZMK and CD4 in serial sections of liver samples from different donors. (H) IF staining of CD4 and GZMK in livers from the 3 types of liver donors. Data are shown in mean  $\pm$  SEM; P-value was obtained by Student's t-test.

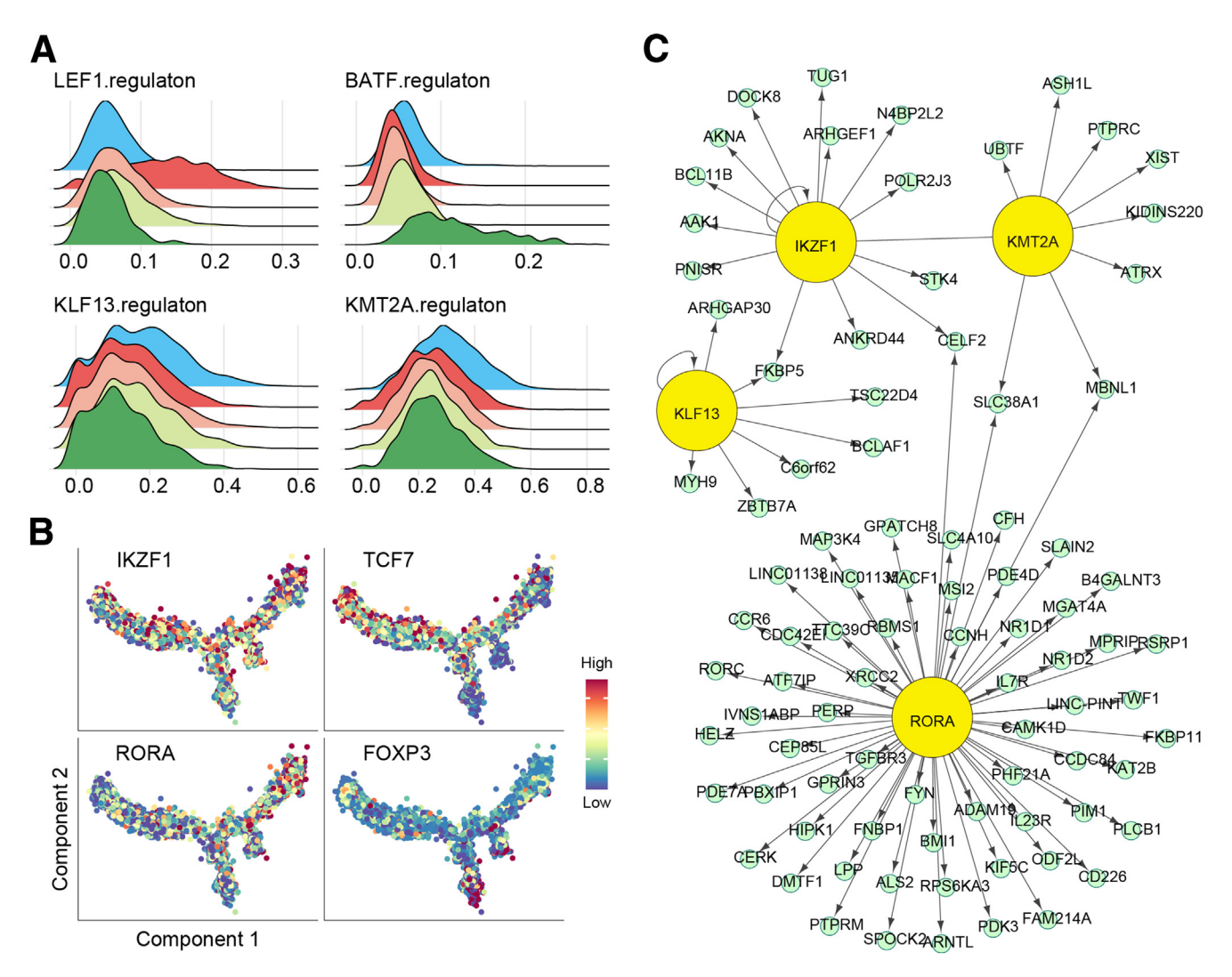


**Figure 9. TFs related to T cell differentiation and functionality.** (A) Heatmap displaying the expression of 4 TFs in the 5 CD4<sup>+</sup> T-cell subsets. (B) UMAP plots showing the expression levels of individual TFs in CD4<sup>+</sup> T-cell subsets. (C) Interaction network highlighting 4 key TFs related to T cell differentiation and functionality.

might have implications for clinical diagnostics and might behave as a potential biomarker in patients with ALD in different disease stages. Our discovery may offer valuable insights for the development of targeted therapeutic interventions in the future.

#### Materials and Methods

## Human Subjects

Fresh samples used in the study were obtained from patients undergoing liver biopsy at Qilu Hospital. A total of 5 patients diagnosed with ALD at Qilu Hospital, Shandong University were enrolled in this study. The liver samples were  $1\times 1$  cm in size, and were processed for scRNA-seq, as described below. For the validation cohort, paraffinembedded tissue sections from controls and MASLD and ALD cohorts were obtained. The study protocol was reviewed and approved by the Ethical Committee of School of Basic Medical Sciences, Shandong University (Document

No. ECSBMSSDU2022-1-40). Informed consent was obtained from all participants.

#### Preparation of Single-cell Suspensions

Each tissue sample was placed in a sterile Petri dish on ice. The tissue was subsequently minced to smaller pieces of less than 3 mm. Sample pieces were transferred to a gentle MACS C Tube (Miltenyi #130-093-237) containing 5 ml digestion enzyme mix. The C tube was then placed on a gentleMACS Octo Dissociator for mechanical dissociation. Upon run completion, the sample was incubated for 30 minutes at 37 °C under continuous low shaking. Subsequently, the sample was filtered using a 70-mm nylon mesh (Miltenyi #130-095-823). Ten ml of this cell suspension was counted by Trypan Blue to determine the concentration of live cells. The sample was then centrifuged at  $300 \times 3$  g and 4 °C for 5 minutes, and the supernatant was discarded. The cell pellet was resuspended in 1 ml freezing media (Gibco). Throughout the dissociation procedure, cells were

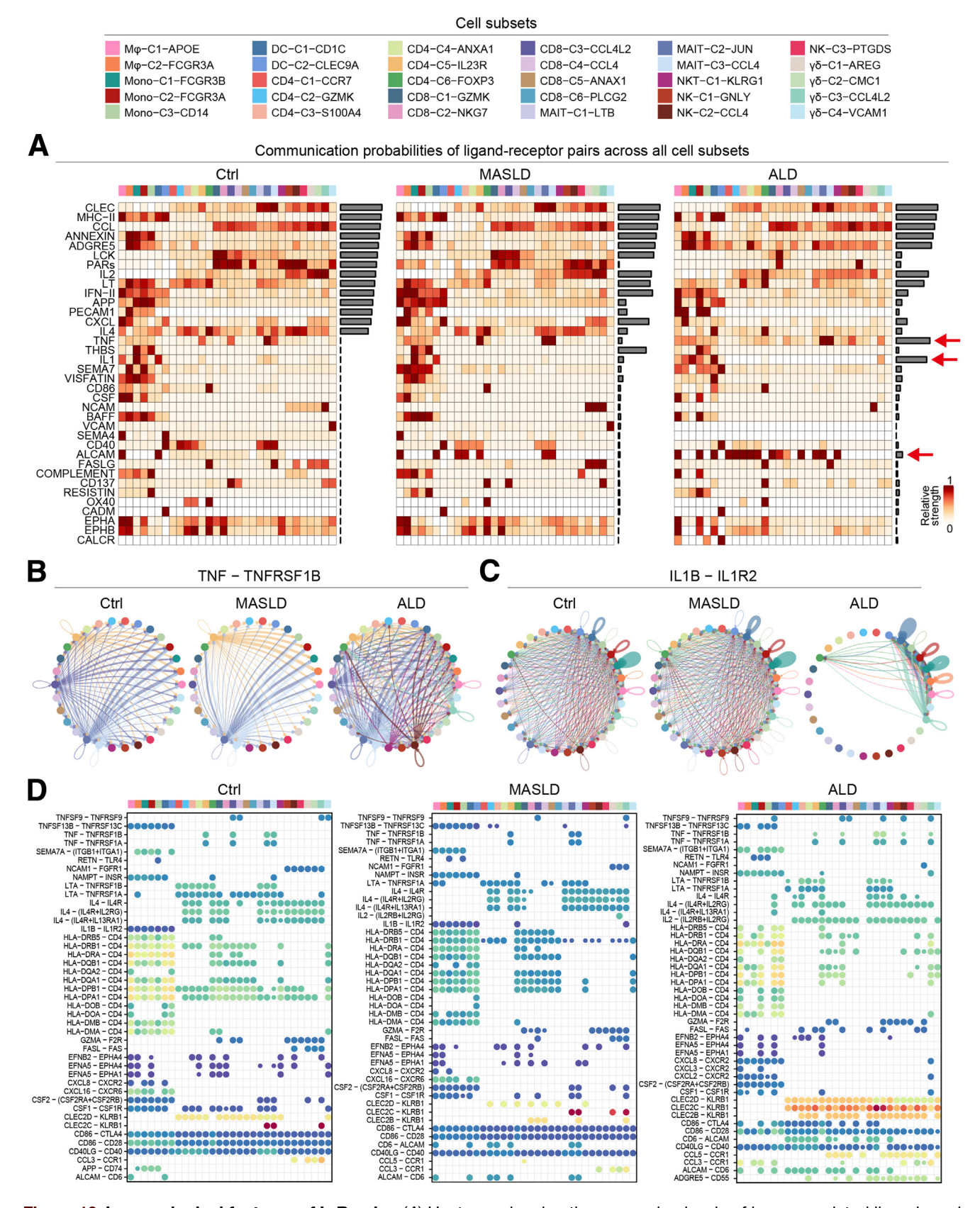


**Figure 10. Immunological features of L-R pairs.** (A) Heatmap showing the expression levels of immune-related ligands and receptors in the livers of different donors. (*B-C*) CSOmap showing the immune-related L-R pairs in liver donors. (*D*) Bubble heatmap showing the L-R pairs in the immune cell subsets in liver donors.

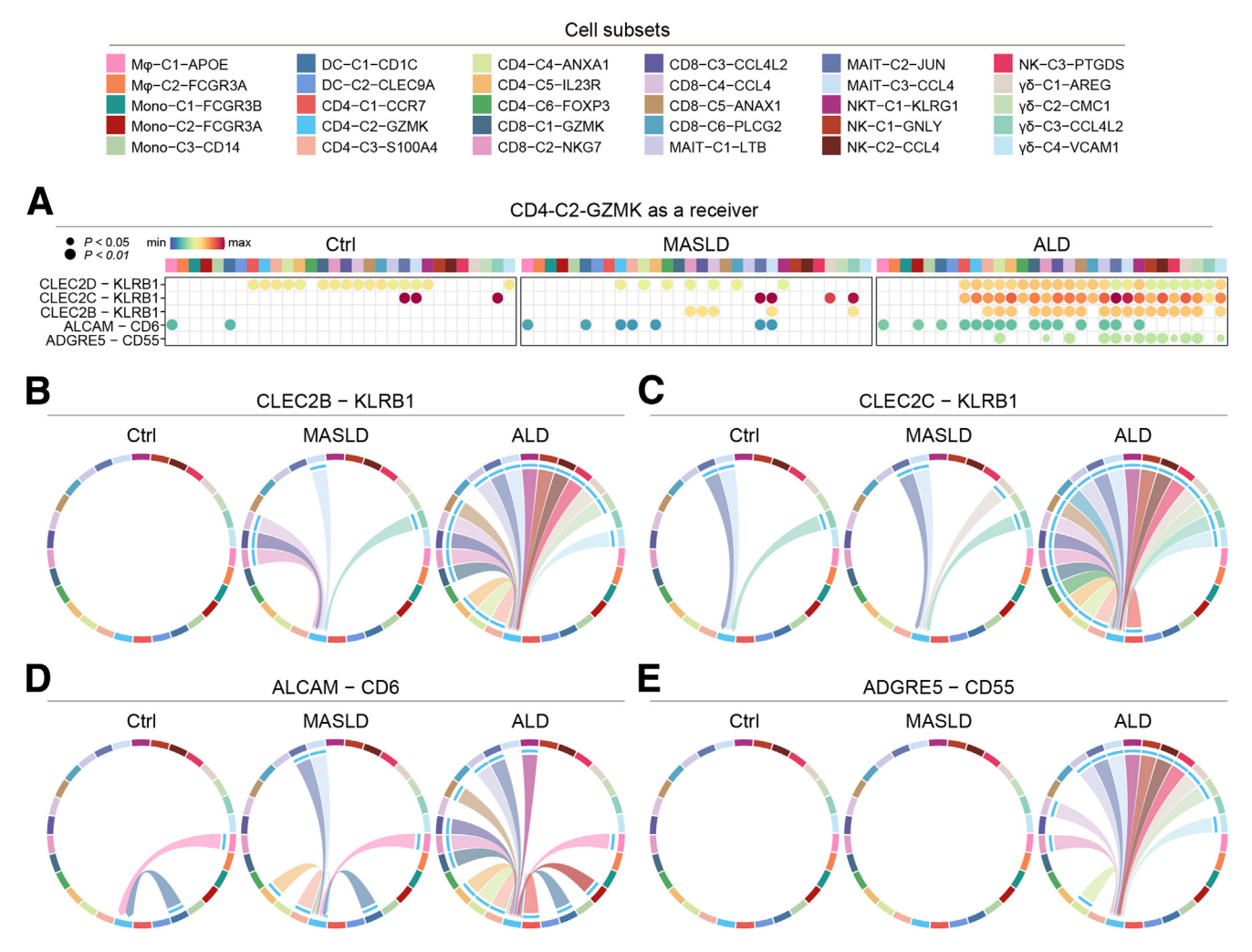


Figure 11. L-R pairs in GZMK+CD4+ T cell subset. (A) Bubble heatmap highlighting the enriched L-R pairs specific to patients with ALD. (B-E) CSOmap showing the correlation of the L-R pairs enriched in patients with ALD in the livers of different donors.

maintained on ice whenever possible, and the entire procedure was completed in less than 1 hour.

# cDNA Library Preparation and Single-cell RNAseq

Single-cell RNA-seq libraries were prepared with Chromium Single cell 30 Reagent v2 Kits according to the manufacturer's protocol. The Chromium Single Cell 30 Library and Gel Bead Kit v2 (PN-120237), Chromium Single Cell 30 Chip kit v2 (PN-120236), and Chromium i7 Multiplex Kit (PN-120262) were used. Briefly, single-cell suspensions were loaded on the Chromium Single Cell Controller Instrument ( $10 \times \text{Genomics}$ ) to generate single-cell gel beads in emulsions (GEMs). After generation of GEMs, reverse transcription reactions were engaged barcoded full-length cDNA followed by the disruption of emulsions using the recovery agent and cDNA clean up with DynaBeads Myone Silane Beads (Thermo Fisher Scientific). cDNA was then amplified by polymerase chain reaction (PCR) with appropriate cycles which depend on the recovery cells.

Subsequently, the amplified cDNA was fragmented, endrepaired, A-tailed, index adaptor ligated, and library amplification. Then these libraries were sequenced on the Illumina sequencing platform (HiSeq X Ten), and 150 bp paired-end reads were generated.

#### Single-cell RNA-seq Data Processing

The Cell Ranger software pipeline (version 2.2.0) provided by  $10 \times Genomics$  was used to demultiplex cellular barcodes, align reads and generate the feature barcode unique molecular identifier (UMI) matrices based on the human reference genome GRCh38. We processed the UMI count matrix using the Seurat R package (v2.4.3). As a quality-control step, the gene expressed less than 1% of cells were discarded. Following visual inspection of the distribution of cells by the fraction of mitochondrial genes expressed, we further discarded low-quality cells where >20% of the counts belonged to mitochondrial genes. Library size normalization was performed in Seurat on the filtered matrix to obtain the normalized count. We

performed principal component analysis (PCA) on the normalized expression matrix using highly variable genes identified by "FindVariableGenes" function. Cells were clustered based on a graph-based clustering approach and were visualized in 2-dimensions using UMAP. Likelihood ratio test that simultaneously test for changes in mean expression and in the percentage of expressed cells was used to identify DEGs between clusters using the Seurat "FindAllMarkers" function. GSEA was performed using the fgsea package in R with the Hallmark gene sets and Reactome pathway. Intercellular communication were analyzed in an unbiased manner using the CellChat package (v1.5.0) to identify significant ligand-receptor pairs within healthy, ALD, and MASLD samples.

## Cell Developmental Trajectory

The cell lineage trajectory of  $CD4^+$  T was inferred by using Monocle2. We used the "differentialGeneTest" function to derive DEG from each cluster and genes with a q-value  $< 1e^{-5}$  were used to order the cells in pseudotime analysis. After the cell trajectories were constructed, DEGs along the pseudotime were detected using the "differentialGeneTest" function.

#### Histology Staining

Mouse livers were removed, fixed overnight in 4% formalin and processed for paraffin embedding. Tissue sections were stained with hematoxylin and eosin (H&E) using standard reagents and protocols. For IHC staining, slides were de-paraffinized, rehydrated, and boiled in a microwave for 10 minutes in 10 mM citrate buffer or Tris-EDTA buffer (according to manufacturer's protocol). The slides were allowed to cool, washed 3 times, incubated with 3% H<sub>2</sub>O<sub>2</sub> to block endogenous peroxidase activity, washed 3 times, and blocked with 5% albumin bovine in IHC wash buffer for 30 minutes. Slides were incubated with primary antibodies overnight at 4 °C, including Anti-CD4 (1:500, (1:20000, Cat#67786-1-Ig, Proteintech), anti-CD8a Cat#66868-1-Ig, Proteintech), anti-GZMK (1:200,Cat#ab282703, Abcam), and anti-NCR1 (1:400,Cat#ab224703, Abcam). The next day, slides were washed 3 times and incubated with horseradish peroxidase (HRP)linked secondary antibodies for 1 hour at room temperature. Specimens were washed 3 times then developed with the DAB substrate kit (ZLI-9018, ZSGB-BIO) and counterstained with hematoxylin.

#### IF Staining

For IF staining, slides were de-paraffinized, rehydrated, and boiled in a microwave for 12 minutes in Tris-EDTA buffer (pH 9.0). The slides were allowed to cool, washed 3 times, and treated with 5% albumin bovine for 30 minutes at room temperature. Slides were incubated with primary antibodies overnight at 4 °C, including anti-CD4 (1:200, Cat#67786-1-Ig, Proteintech), anti-GZMK (1:100, Cat#ab282703, Abcam), anti-CD8 (1:200, Cat#66868-1-Ig, Proteintech), anti-NKG7 (1:200, Cat#84835, CST), anti-ANXA1 (1:200, Cat#32934, CST). The next day, slides

were washed 3 times and incubated with HRP-linked secondary antibodies for 1 hour at room temperature. the corresponding secondary antibodies (goat anti-mouse Alexa 488 [1:400] and/or goat anti-rabbit Alexa 594 [1:400]) for 1 hour at room temperature. Nuclei were visualized with 4,6-diamidino-2-phenylindole (DAPI) staining before the sections were covered with coverslips.

## Statistical Analysis

Statistical significance was assessed by 2-tailed unpaired Student t-test, 1-way analysis of variance (ANOVA) followed by Fisher's least significant difference (LSD) test or Wilcoxon rank-sum test, as indicated in the figure legends. Statistical analysis was performed using GraphPad Prism 7 (GraphPad Software). P values < .05 were considered significant.

#### References

- Bataller R, Arab JP, Shah VH. Alcohol-associated hepatitis. N Engl J Med 2022;387:2436–2448.
- Wen B, Zhang C, Zhou J, et al. Targeted treatment of alcoholic liver disease based on inflammatory signalling pathways. Pharmacol Ther 2021;222:107752.
- Hosseini N, Shor J, Szabo G. Alcoholic hepatitis: a review. Alcohol Alcohol 2019;54:408–416.
- Arab JP, Izzy M, Leggio L, et al. Management of alcohol use disorder in patients with cirrhosis in the setting of liver transplantation. Nat Rev Gastroenterol Hepatol 2022;19:45–59.
- Singal AK, Shah VH. Current trials and novel therapeutic targets for alcoholic hepatitis. J Hepatol 2019; 70:305–313.
- Rodriguez WE, Wahlang B, Wang Y, et al. Phosphodiesterase 4 inhibition as a therapeutic target for alcoholic liver disease: from bedside to bench. Hepatology 2019; 70:1958–1971.
- Cho Y, Bukong TN, Tornai D, et al. Neutrophil extracellular traps contribute to liver damage and increase defective low-density neutrophils in alcohol-associated hepatitis. J Hepatol 2023;78:28–44.
- Saha B, Momen-Heravi F, Furi I, et al. Extracellular vesicles from mice with alcoholic liver disease carry a distinct protein cargo and induce macrophage activation through heat shock protein 90. Hepatology 2018; 67:1986–2000.
- Effenberger M, Widjaja AA, Grabherr F, et al. Interleukin-11 drives human and mouse alcohol-related liver disease. Gut 2023;72:168–179.
- Wang M, You Q, Lor K, et al. Chronic alcohol ingestion modulates hepatic macrophage populations and functions in mice. J Leukoc Biol 2014;96:657–665.
- Saha B, Bala S, Hosseini N, et al. Krüppel-like factor 4 is a transcriptional regulator of M1/M2 macrophage polarization in alcoholic liver disease. J Leukoc Biol 2015;97:963–973.
- 12. Gao B, Ma J, Xiang X. MAIT cells: a novel therapeutic target for alcoholic liver disease? Gut 2018;67:784–786.
- Renand A, Cervera-Marzal I, Gil L, et al. Integrative molecular profiling of autoreactive CD4 T cells in autoimmune hepatitis. J Hepatol 2020;73:1379–1390.

- Ramachandran P, Dobie R, Wilson-Kanamori JR, et al. Resolving the fibrotic niche of human liver cirrhosis at single-cell level. Nature 2019;575:512–518.
- Sun Y, Wu L, Zhong Y, et al. Single-cell landscape of the ecosystem in early-relapse hepatocellular carcinoma. Cell 2021;184:404–421.e16.
- Woestemeier A, Scognamiglio P, Zhao Y, et al. Multicytokine-producing CD4+ T cells characterize the livers of patients with NASH. JCI Insight 2023;8:e153831.
- Browaeys R, Saelens W, Saeys Y. NicheNet: modeling intercellular communication by linking ligands to target genes. Nat Methods 2020;17:159–162.
- 18. Morrison JK, DeRossi C, Alter IL, et al. Single-cell transcriptomics reveals conserved cell identities and fibrogenic phenotypes in zebrafish and human liver. Hepatol Commun 2022;6:1711–1724.
- Su Q, Kim SY, Adewale F, et al. Single-cell RNA transcriptome landscape of hepatocytes and non-parenchymal cells in healthy and NAFLD mouse liver. Iscience 2021;24:103233.
- Zhang C, Li J, Cheng Y, et al. Single-cell RNA sequencing reveals intrahepatic and peripheral immune characteristics related to disease phases in HBVinfected patients. Gut 2023;72:153–167.
- Pfister D, Núñez NG, Pinyol R, et al. NASH limits antitumour surveillance in immunotherapy-treated HCC. Nature 2021;592:450–456.
- Villani AC, Satija R, Reynolds G, et al. Single-cell RNAseq reveals new types of human blood dendritic cells, monocytes, and progenitors. Science 2017;356: eaah4573.
- 23. Ramírez-Pérez O, Barranco-Fragoso B, Pichardo-Bahena R, et al. The role of dendritic cells in different stages of non-alcoholic fatty liver disease. J Hepatol 2018;68:S363–S364.
- Haas JT, Vonghia L, Mogilenko DA, et al. Transcriptional network analysis implicates altered hepatic immune function in NASH development and resolution. Nat Metab 2019;1:604–614.
- Ramadori P, Kam S, Heikenwalder M. T cells: friends and foes in NASH pathogenesis and hepatocarcinogenesis. Hepatology 2022;75:1038–1049.
- MacParland SA, Liu JC, Ma XZ, et al. Single cell RNA sequencing of human liver reveals distinct intrahepatic macrophage populations. Nat Commun 2018;9:4383.
- 27. Rouland A, Masson D, Lagrost L, et al. Role of apolipoprotein C1 in lipoprotein metabolism, atherosclerosis and diabetes: a systematic review. Cardiovasc Diabetol 2022;21:272.
- Li F, Zhang HR. Lysosomal acid lipase in lipid metabolism and beyond. Arterioscler Thromb Vasc Biol 2019; 39:850–856.
- 29. Herrera-Marcos LV, Martínez-Beamonte R, Macías-Herranz M, et al. Hepatic galectin-3 is associated with lipid droplet area in non-alcoholic steatohepatitis in a new swine model. Sci Rep 2022;12:1024.
- **30.** Jaitin DA, Adlung L, Thaiss CA, et al. Lipid-associated macrophages control metabolic homeostasis in a Trem2-dependent manner. Cell 2019;178:686–698.e14.

- Kapellos TS, Bonaguro L, Gemund I, et al. Human monocyte subsets and phenotypes in major chronic inflammatory diseases. Front Immunol 2019;10:2035.
- 32. Nassir N, Tambi R, Bankapur A, et al. Single-cell transcriptome identifies FCGR3B upregulated subtype of alveolar macrophages in patients with critical COVID-19. iScience 2021;24:103030.
- van den Brink SC, Sage F, Vertesy A, et al. Single-cell sequencing reveals dissociation-induced gene expression in tissue subpopulations. Nat Methods 2017; 14:935–936.
- 34. Dudek M, Pfister D, Donakonda S, et al. Auto-aggressive CXCR6(+) CD8 T cells cause liver immune pathology in NASH. Nature 2021;592:444–449.
- 35. Chowdhury RR, Valainis JR, Kask O, et al. The role of antigen recognition in the  $\gamma\delta$  T cell response at the controlled stage of M. tuberculosis infection. bioRxiv 2021.
- **36.** Ma C, Kesarwala AH, Eggert T, et al. NAFLD causes selective CD4(+) T lymphocyte loss and promotes hepatocarcinogenesis. Nature 2016;531:253–257.
- 37. Park S, Griesenauer B, Jiang H, et al. Granzyme A-producing T helper cells are critical for acute graft-versushost disease. JCI Insight 2020;5:124465.
- 38. Mackay LK, Minnich M, Kragten NA, et al. Hobit and Blimp1 instruct a universal transcriptional program of tissue residency in lymphocytes. Science 2016; 352:459–463.
- 39. Han L, Chen S, Chen Z, et al. Interleukin 32 promotes Foxp3(+) Treg cell development and CD8(+) T cell function in human esophageal squamous cell carcinoma microenvironment. Front Cell Dev Biol 2021;9:704853.
- Aibar S, Gonzalez-Blas CB, Moerman T, et al. SCENIC: single-cell regulatory network inference and clustering. Nat Methods 2017;14:1083–1086.
- Kwon SJ, Crespo-Barreto J, Zhang W, et al. KLF13 cooperates with c-Maf to regulate IL-4 expression in CD4+ T cells. J Immunol 2014;192:5703–5709.
- 42. Li H, van der Leun AM, Yofe I, et al. Dysfunctional CD8 T cells form a proliferative, dynamically regulated compartment within human melanoma. Cell 2019; 176:775–789.e18.
- 43. Yamashita M, Hirahara K, Shinnakasu R, et al. Crucial role of MLL for the maintenance of memory T helper type 2 cell responses. Immunity 2006;24:611–622.
- 44. Jin S, Guerrero-Juarez CF, Zhang L, et al. Inference and analysis of cell-cell communication using CellChat. Nat Commun 2021;12:1088.
- 45. Fergusson JR, Fleming VM, Klenerman P. CD161-expressing human T cells. Front Immunol 2011;2:36.
- Konduri V, Oyewole-Said D, Vazquez-Perez J, et al. CD8(+)CD161(+) T-Cells: cytotoxic memory cells with high therapeutic potential. Front Immunol 2020;11: 613204.
- Mathewson ND, Ashenberg O, Tirosh I, et al. Inhibitory CD161 receptor identified in glioma-infiltrating T cells by single-cell analysis. Cell 2021;184:1281–1298.e26.
- 48. Hashimoto K, Kouno T, Ikawa T, et al. Single-cell transcriptomics reveals expansion of cytotoxic CD4 T cells in

- supercentenarians. Proc Natl Acad Sci U S A 2019; 116:24242-24251.
- Rambaldi B, Kim HT, Arihara Y, et al. Phenotypic and functional characterization of the CD6-ALCAM T-cell costimulatory pathway after allogeneic cell transplantation. Haematologica 2022;107:2617–2629.
- Chalmers SA, Ayilam Ramachandran R, Garcia SJ, et al. The CD6/ALCAM pathway promotes lupus nephritis via T cell-mediated responses. J Clin Invest 2022;132: e147334.
- Capasso M, Durrant LG, Stacey M, et al. Costimulation via CD55 on human CD4+ T cells mediated by CD97. J Immunol 2006;177:1070–1077.
- Sutavani RV, Bradley RG, Ramage JM, et al. CD55 costimulation induces differentiation of a discrete T regulatory type 1 cell population with a stable phenotype. J Immunol 2013;191:5895–5903.
- Grazia TJ, Plenter RJ, Weber SM, et al. Acute cardiac allograft rejection by directly cytotoxic CD4 T cells: parallel requirements for Fas and perforin. Transplantation 2010;89:33–39.
- 54. Maehara T, Kaneko N, Perugino CA, et al. Cytotoxic CD4+ T lymphocytes may induce endothelial cell apoptosis in systemic sclerosis. J Clin Invest 2020; 130:2451–2464.
- 55. Sacher AG, St Paul M, Paige CJ, et al. Cytotoxic CD4(+) T cells in bladder cancer-a new license to kill. Cancer Cell 2020;38:28–30.
- 56. Oh DY, Kwek SS, Raju SS, et al. Intratumoral CD4(+) T cells mediate anti-tumor cytotoxicity in human bladder cancer. Cell 2020;181:1612–1625.e13.
- Li S, Tan H-Y, Wang N, et al. Recent insights into the role of immune cells in alcoholic liver disease. Front Immunol 2019;10:1328.
- 58. Pan Hn, Sun R, Jaruga B, et al. Chronic ethanol consumption inhibits hepatic natural killer cell activity and accelerates murine cytomegalovirus-induced hepatitis. Alcohol Clin Exp Res 2006;30:1615–1623.
- Stoy S, Dige A, Sandahl TD, et al. Cytotoxic T lymphocytes and natural killer cells display impaired cytotoxic functions and reduced activation in patients with alcoholic hepatitis. Am J Physiol Gastrointest Liver Physiol 2015;308:G269–G276.
- Laso FJ, Madruga JI, Lopez A, et al. Abnormalities of peripheral blood T lymphocytes and natural killer cells in alcoholic hepatitis persist after a 3-month withdrawal period. Alcohol Clin Exp Res 1997;21:672–676.
- 61. Laso FJ, Almeida J, Torres E, et al. Chronic alcohol consumption is associated with an increased cytotoxic profile of circulating lymphocytes that may be related with the development of liver injury. Alcohol Clin Exp Res 2010;34:876–885.
- Cheng Y, Zhu Y, Xu J, et al. PKN2 in colon cancer cells inhibits M2 phenotype polarization of tumor-associated macrophages via regulating DUSP6-Erk1/2 pathway. Mol Cancer 2018;17:13.
- Guilliams M, Bonnardel J, Haest B, et al. Spatial proteogenomics reveals distinct and evolutionarily conserved hepatic macrophage niches. Cell 2022; 185:379–396.e38.

- 64. Remmerie A, Martens L, Thone T, et al. Osteopontin expression identifies a subset of recruited macrophages distinct from Kupffer cells in the fatty liver. Immunity 2020;53:641–657.e14.
- 65. Nalio Ramos R, Missolo-Koussou Y, Gerber-Ferder Y, et al. Tissue-resident FOLR2(+) macrophages associate with CD8(+) T cell infiltration in human breast cancer. Cell 2022;185:1189–1207.e25.
- Liu C, Martins AJ, Lau WW, et al. Time-resolved systems immunology reveals a late juncture linked to fatal COVID-19. Cell 2021;184:1836–1857.e22.
- Rao M, Wang X, Guo G, et al. Resolving the intertwining of inflammation and fibrosis in human heart failure at single-cell level. Basic Res Cardiol 2021; 116:55.
- 68. Bai Y-M, Liang S, Zhou B. Revealing immune infiltrate characteristics and potential immune-related genes in hepatic fibrosis: based on bioinformatics, transcriptomics and q-PCR experiments. Front Immunol 2023;14:1133543.
- 69. Satija R, Farrell JA, Gennert D, et al. Spatial reconstruction of single-cell gene expression data. Nature biotechnology 2015;33(5):495–502.

#### Received November 16, 2023. Accepted September 23, 2024.

#### Correspondence

Address correspondence to: Cuijuan Zhang, Institute of Pathology and Pathophysiology, Cheeloo College of Medicine, Shandong University, Jinan 250012, China. e-mail: cuijuanzhang@sdu.edu.cn; or Detian Yuan, Department of Biochemistry and Molecular Biology, School of Basic Medical Sciences, Cheeloo College of Medicine, Shandong University, Jinan 250012, China. e-mail: yuandt@sdu.edu.cn; Mathias Heikenwalder, University Tuebingen, Faculty of Medicine, Institute for Interdisciplinary Research on Cancer Metabolism and Chronic Inflammation, M3-Research Center for Malignome, Metabolome and Microbiome, Otfried-Müller-Straße 37, 72076 Tübingen, Germany. e-mail: m.heikenwaelder@dkfz-heidelberg.de; or Peng Zhang, Department of Biochemistry and Molecular Biology, School of Basic Medical Sciences, Cheeloo College of Medicine, Shandong University, Jinan 250012, China. e-mail: zhangpeng1990@sdu.edu.cn.

#### Acknowledgments

The authors thank the technical assistance at the Core facility of Advanced Medical Research Institute of Shandong University.

#### **CRediT Authorship Contributions**

Chao Gao (Data curation: Lead; Investigation: Lead)

Shiguan Wang (Data curation: Equal; Funding acquisition: Supporting; Investigation: Equal)

Xiaoyu Xie (Data curation: Equal; Funding acquisition: Equal; Investigation: Equal; Writing – original draft: Equal)

Pierluigi Ramadori (Investigation: Equal; Writing - review & editing: Equal)

Xinying Li (Data curation: Equal; Investigation: Equal)

Xiaoyu Liu (Methodology: Supporting) Xue Ding (Methodology: Supporting)

Jinyuan Liang (Methodology: Supporting) Bowen Xu (Methodology: Supporting)

Yawei Feng (Methodology: Supporting) Xueying Tan (Methodology: Supporting) Haoran Wang (Methodology: Supporting)

Yan Zhang (Methodology: Supporting)
Haiyan Zhang (Methodology: Supporting)

Tingguo Zhang (Funding acquisition: Equal; Methodology: Supporting)
Ping Mi (Funding acquisition: Equal; Methodology: Supporting)

Shiyang Li (Funding acquisition: Equal; Methodology: Supporting)

Cuijuan Zhang (Funding acquisition: Equal; Methodology: Supporting; Writing – review & editing: Equal)

Detian Yuan (Conceptualization: Lead; Funding acquisition: Equal; Supervision: Lead; Writing - original draft: Lead; Writing - review & editing: Lead)

Mathias Heikenwälder (Conceptualization: Equal; Writing – review & editing: Equal)

Peng Zhang (Data curation: Lead; Funding acquisition: Equal; Investigation: Equal; Writing – original draft: Equal; Writing – review & editing: Equal)

#### **Conflicts of interest**

The authors disclose no conflicts.

#### Funding

This work was supported by National Key Research and Development Program of China to Shiyang Li (2020YFA0804400); National Natural Science Foundation of China (82270621, 32422024, 82071854, 82200643, 32100590, 32270820); Natural Science Foundation of Shandong Province (ZR2020QH038, ZR2022QH092, ZR2021QB012, ZR2022MH150, ZR2020MH269, ZR2016HP07); Shandong Province Medical and Health Technology Development Project (2017WS032); Funds for Youth Interdisciplinary and Innovation Research Groups of Shandong University (2020QNQT003 and 2020QNQT009); the Fundamental Research Funds for

the Central Universities (2022JC008); the China Postdoctoral Innovation Talent Support Program to Shiguan Wang (BX20230211); the European Commission (Horizon Europe-Mission Cancer, THRIVE, ref. 101136622) (Mathias Heikenwalder); SFB 1479 (project ID: 441891347) (Mathias Heikenwalder); SFB/TR 179 (project ID: 272983813) (Mathias Heikenwalder); The Rainer Hoenig Stiftung (Mathias Heikenwalder); Research Foundation Flanders (FWO) under grant 30826052 (EOS Convention MODEL-IDI) (Mathias Heikenwalder).

#### **Data Availability**

The scRNA-seq data presented in this study have been submitted to the GEO database and are available under accession number GSE236382 for samples from patients with ALD, and under accession number GSE159977 for samples from healthy donors and individuals with MASLD. All codes and scripts used for association studies are available on request.